

# Activity of ordered and disordered Pt-Co alloy phases for the electroreduction of oxygen in catalysts with multiple coexisting phases

Shirlaine Koh, Chengfei Yu, Prasanna Mani, Ratndeeep Srivastava, Peter Strasser\*

*Department of Chemical and Biomolecular Engineering, University of Houston, Houston, TX 77204-4004, USA*

Received 25 October 2006; received in revised form 2 January 2007; accepted 3 January 2007

Available online 13 January 2007

## Abstract

This study investigates the relative electrochemical activity of ordered and disordered Pt-Co alloy phases coexisting in multi-phase catalyst materials. Of particular interest is the effect of the relative distribution between ordered and disordered Pt-Co alloy phases on the observed electrocatalytic activity for the oxygen reduction reaction (ORR). Three Pt-Co catalysts with identical overall composition, Pt<sub>50</sub>Co<sub>50</sub>, but with distinct distributions between two disordered face centered cubic (fcc) Pt-Co alloy phases and one ordered face centered tetragonal (fct) alloy phase are considered. Comparing the structure of the catalysts with their electrocatalytic activity for ORR suggests that the Co-rich (60–80 at% Co) disordered phase is linked to the observed 3× activity enhancement compared to a pure Pt catalyst. If the ordered fct phase outweighs the Co-rich disordered phase the activity drops drastically. It is concluded that Co-rich disordered phases are the preferred Pt-Co alloy phases with respect to catalyst activity.

© 2007 Elsevier B.V. All rights reserved.

*Keywords:* Metal alloys; Fuel cell catalysis; Oxygen reduction reaction; Synthesis–property relationship; Kinetic measurements

## 1. Introduction

Hydrogen/oxygen polymer-electrolyte-membrane fuel cells (PEMFCs) suffer from severe cell potential losses at the Pt cathode electrocatalysts where molecular oxygen and protons are electroreduced to water in a complex multi-step reaction sequence. At moderate current densities, the overpotentials are mainly caused by kinetic barriers associated with surface adsorption and reductive charge transfer processes on the catalyst surface. Despite a large body of literature over the past decades on improved ORR electrocatalysts, the search of more active electrocatalysts with less Pt content continues to be a scientific priority in fuel cell catalysis research. Pt alloy electrocatalysts have been receiving much attention over the years [1]. Recently, Co containing Pt alloys [2–5] have become a focus in PEMFC cathode electrocatalysis [6–13]. There is consensus that Pt-Co alloys offer a favorable intrinsic enhancement. For well-defined smooth Pt<sub>50</sub>Co<sub>50</sub> alloy surfaces at 900 mV/RHE and 60 C under rotating disk electrode conditions, an improve-

ment factor in Pt surface area based ORR activity (specific electrocatalytic activity) of about 3–4× was reported [11,14,15]. For carbon-supported high surface area Pt<sub>50</sub>Co<sub>50</sub> particle alloys, Pt mass based activity enhancements of 1.5–2× were reported at 900 mV/RHE [11,14], while specific activity enhancements ranged around 2–3× [11,16,17]. The absolute values of the specific activity enhancements vary by orders of magnitude [17,15], depending on the format of the electrocatalysts. This is thought to be associated with a so-called particle size effect [17]. For Pt<sub>50</sub>Co<sub>50</sub> alloy particles at 900 mV/RHE reported values range at around 550 μA cm<sup>-2</sup><sub>Pt</sub> in Pt surface area based activity.

Studies involving well-defined Pt-Co alloy surfaces have typically addressed the relation between surface structure, surface composition and electrocatalytic activity [11,14–16]. A ‘Pt skin’ structure, obtained after high temperature annealing, was found to be more active than a ‘sputtered’ surface [15]. Studies on Pt-Co nanoparticle catalysts, in contrast, have mainly focused on the structure of the alloy bulk (lattice constants, unit cell symmetry, etc.) of the alloy phases [6,7,12,18–27].

Most previous structural studies on Pt-Co particle electrocatalysts reported the presence of a single ordered or disordered alloy phase. Careful inspection of some of the reported X-ray

\* Corresponding author. Tel.: +1 713 743 4310; fax: +1 713 743 4323.

E-mail address: [pstrasser@uh.edu](mailto:pstrasser@uh.edu) (P. Strasser).

diffraction profiles, however, does indicate shoulders and therefore the possibility of unaddressed coexisting multiple alloy phases [18,27,28]. In many of these studies, alloy particles were prepared stepwise using impregnation of liquid transition metal solutions on commercial Pt precursors consisting of carbon-supported Pt particles. Pt particle precursors with relatively large mean particle size (3–4 nm diameter) combined with annealing temperatures up to 900 °C [12,18] resulted in narrow and very intense reflections hampering the identification of shoulders and multiple coexisting phases. The use of Pt precursors of higher dispersion (1–2 nm Pt mean particle diameter) and moderate annealing temperatures ranging from 600 to 800 °C [26,29–31] rarely produced single phase alloy particles. In these materials, broad, often multiple peaks, indicate multiple ordered and/or disordered alloy phases [26]. Despite the occurrence of multiple alloy phases under such a wide range of synthesis conditions, structure–activity effects associated with multi-phase alloy catalysts have largely remained unaddressed.

In this study, we investigate the effect of the relative distribution of ordered and disordered Pt-Co alloy phases on the observed electrocatalytic activity for the ORR in order to assess their relative electrocatalytic activity. Three Pt-Co catalysts are considered with overall composition Pt<sub>50</sub>Co<sub>50</sub> but with distinct distributions between two disordered face centered cubic (fcc) phases and one ordered face centered tetragonal (fct) phase. We show that the predominant presence of the Co-rich (Co > 60–80 at%) disordered fcc phases is associated with a large three-fold ORR activity enhancement of the catalyst. For larger relative weights of the ordered phase, the activity drops drastically regardless of the relative weight of the Pt rich disordered fcc phase. Our results suggest that Co-rich disordered fcc phases are preferred over the ordered fct phase when it comes to optimizing the electrochemical ORR activity [25].

## 2. Experimental

### 2.1. Catalyst synthesis

Three Pt-Co alloy nanoparticle catalysts with an overall stoichiometry of Pt<sub>50</sub>Co<sub>50</sub>, referred to as catalyst ‘1’, ‘2’, and ‘3’, were prepared via the following procedures.

#### 2.1.1. Pt-Co catalyst 1

This catalyst was synthesized by adding appropriate amounts of solid Co precursor (Co(NO<sub>3</sub>)<sub>2</sub>·6H<sub>2</sub>O, Sigma Aldrich #239267) to 0.2 g of a powder electrocatalysts consisting of about 30 wt% platinum supported on a high surface area carbon support. De-ionized water (>18.2 MΩ, Millipore Gradient System) was added to the supported catalyst powder and the mixture was ultrasonicated for 1 min (Branson Sonifier 150) until a thick slurry formed. The catalyst synthesis mixture was subsequently frozen in liquid nitrogen, and then freeze-dried in vacuum (50 mTorr) overnight until the temperature of the sample reached 25 °C. The resulting catalyst precursor powder was distributed evenly into two small quartz vials of 1 in. diameter and 1.2 in. height. The quartz vials containing the powders were then placed in the center of a 3 feet long quartz tube (3 in.

diameter) in the flow furnace (Lindberg Blue). The powders were then annealed to a maximum temperature of 600 °C for 7 h (10 K min<sup>-1</sup> heating rate) under a flowing 4% hydrogen atmosphere (Ar balance) and slowly cooled down without any forced convection. The final Pt weight loadings of the Pt-Co alloys were about 26 wt % Pt.

#### 2.1.2. Pt-Co catalyst 2

Synthesis followed very closely that of catalyst 1, using similar amounts of the Co precursor, carbon-supported Pt precursor as well as amount of de-ionized water. Duration and conditions of the ultrasonication, freeze-drying and annealing processes were also kept very close to those of catalyst 1.

#### 2.1.3. Pt-Co catalyst 3

This synthesis followed that of catalysts 1 and 2 with some modifications. A Co precursor solution was prepared first by adding appropriate amount of Co(NO<sub>3</sub>)<sub>2</sub>·6H<sub>2</sub>O to de-ionized water (grade see above); this solution was ultrasonicated for 1 min. Then, a weighed amount of powder electrocatalysts consisting of about 30 wt% platinum supported on a high surface area carbon was added to the Co precursor solution. This catalyst-Co precursor mixture was ultrasonicated for 1 min followed by 1 min cooling and again 1 min sonication to form thick slurry (Branson Sonifier 150). The catalyst synthesis mixture was subsequently frozen in liquid nitrogen (5 min), and then freeze-dried in vacuum (50 mTorr) until the temperature of the sample reaches 25 °C. The resulting powder was loaded as a thin powder film on the bottom of a rectangular alumina boat (50 mL) with a partially covering lid. The sample was annealed to a maximum temperature of 600 °C for 7 h under 4% hydrogen atmosphere (Ar balance) at the same flow rate as catalysts 1 and 2 and cooled down at about 3 K min<sup>-1</sup>.

### 2.2. Electrode film preparation

Rotating disk powder catalyst electrode preparation followed procedures published earlier [17,32]. Prior to electrode preparation, a 5 mm diameter glassy carbon rotating disk electrode (RDE) was polished to a mirror finish using 0.5 and 0.05 μm alumina suspension (Buehler Inc.). A catalyst ink was prepared by mixing the catalyst powder in 20 mL of an aqueous solution (>18.2 MΩ, Millipore Gradient System) containing 5 wt% Nafion<sup>®</sup> solution (Sigma, #274704). A 10 μL aliquot was dispensed onto the rotating disk electrode resulting in a typically Pt loading of about 14 μg Pt cm<sup>-2</sup> geometric surface area. The ink was then dried for 10 min in air.

### 2.3. Electrochemical measurement

The electrochemical cell was a custom-made, three-compartment cell. The working electrode was a commercial glassy carbon rotating disk electrode of 5 mm fixed diameter. The reference electrode was a mercury–mercury sulphate electrode. All electrode potentials were subsequently converted into and are reported with respect to the reversible hydrogen electrode (RHE) scale. The counter electrode was a piece of

platinum gauze to ensure large surface area. A commercial rotator from Pine Instrument was used to conduct the rotating disk experiment. The electrolyte used was 0.1 M HClO<sub>4</sub>, prepared by diluting 70% redistilled HClO<sub>4</sub> (Sigma #311421) with deionized water (>18.2 MΩ, Millipore Gradient System). The disk potential was controlled with a potentiostat, BiStat (Princeton Applied Research, Ametek). All measurements were conducted at room temperature. At the beginning of electrochemical measurements, electrocatalysts were immersed into the electrolyte under potential control and held at 0.06 V/RHE until the measurements commenced.

Cyclic voltammetric (CV) measurements were conducted in de-aerated electrolyte, under N<sub>2</sub> atmosphere. The electrocatalyst were first pretreated using 200 CV scans between 0.06 and 1.2 V at a scan rate of 500 mV s<sup>-1</sup>. Thereafter, the potential was scanned at 100 mV s<sup>-1</sup> from 0.06 to 1.2 V and back to 0.06 V. The electrochemical platinum surface area (Pt-ESA) of the catalyst was determined from the mean integral charge of the hydrogen adsorption and desorption areas after double-layer correction, using 210 μC/cm<sup>2</sup> (Pt) [33] as the conversion factor.

Linear sweep voltammetry (LSV) measurements were conducted by sweeping the potential from 0.06 V anodically to the open circuit potential (around 1.0 V) at the scan rate of 5 mV s<sup>-1</sup>. Mass and specific activities were established at 900 mV/RHE, at room temperature. The electrochemical behavior (CV and LSV) of the Pt-Co catalysts was compared to a 30 wt% reference platinum electrocatalyst supported on a high surface area carbon support.

#### 2.4. X-ray diffraction (XRD)

All XRDs of the Pt-Co catalysts were recorded under identical conditions using identical specimen thicknesses. XRD was conducted using a Siemens D5000 ( $\theta/2\theta$ ) Diffractometer equipped with a Braun Position Sensitive Detector (PSD) with an angular range of 8°. The Cu K $\alpha$  source was operating at a potential of 35 kV and a current of 30 mA.  $2\theta$  diffraction angles ranged from 21° to 70°, using step scans of 0.02° per step and a holding time of 10 s per step. Advanced X-ray Solution (X-ray commander, Bruker AXS) software was used to control the diffractometer from a desktop computer. Composition estimation of disordered Pt-Co alloy phases (substitutional solid solutions) was based on the linear relationship between molar Co content and size of resulting lattice parameters [34,35]. All X-ray diffraction patterns were analyzed using Jade 7.5 of Material Data, Inc. (MDI): peak profiles of individual reflections were obtained by a non-linear least-square fit of the Cu K $\alpha_2$  corrected data. Instrumental broadening was determined by a standard powder sample under identical measurement conditions.

### 3. Results and discussion

#### 3.1. Alloy phase formation during reductive annealing

Given their commercial availability, highly dispersed carbon-supported Pt particle precursor catalysts have become a popular starting material for the preparation of carbon sup-

ported high surface area alloy nanoparticles via impregnation–drying–annealing synthesis routes [6,7,23,12,36]. By eliminating the Pt deposition step the synthesis process is simplified and takes advantage of the high initial dispersion of commercially prepared Pt/C catalysts. Compared to typical wet-chemical reduction/alloying methods [37–42], where the alloy constituents are atomically mixed prior to reduction, the kinetics of alloy formation during solid state reductive annealing is governed by the mobility and diffusion coefficients of the metal particles and the individual Pt and Co atoms, respectively. We speculate that at the beginning of the reductive annealing process, the crystalline Pt phases of the precursor material typically coexist with relatively large amorphous Co salt phases. In the course of the annealing, the salt anion decomposes (most nitrates decompose at 250–350 °C), and Co-oxide phases are reduced to form relatively large metallic Co particles [43]. Co atoms randomly diffuse into the Pt particle lattices and most likely form a distribution of disordered (random) Pt-Co alloy phases of varying composition. Eventually, under extended annealing, the thermodynamically most stable alloy phase distribution at the chosen temperature will form. For the annealing temperature of the Pt-Co alloys chosen here (600 °C), the formation of an ordered Pt<sub>50</sub>Co<sub>50</sub> phase is thermodynamically favored [12]. However, the nucleation and growth of the ordered phase is slow at 600 °C so that a distribution of ordered and disordered phases emerges [12,44,45]. The complexity of the solid state processes involved in the solid state alloy preparation explains why minute variations in annealing conditions may significantly affect the resulting compositional distribution of Pt-Co alloy phases.

#### 3.2. Pt-Co alloy phase distribution in nanoparticle catalysts with multiple phases

Three carbon-supported high surface area Pt-Co nanoparticle electrocatalysts with the overall stoichiometry Pt<sub>50</sub>Co<sub>50</sub> (catalysts ‘1’, ‘2’, and ‘3’) were prepared using a recently described impregnation–freeze–drying–reductive annealing method [25,26,43]. Fig. 1a–c shows the XRD profile of the catalysts ‘1’, ‘2’, and ‘3’, respectively.

Peak profile analysis and crystallographic data of the individual phases are summarized in Table 1. Each catalyst consists of a very similar set of three compositionally distinct Pt-Co alloy phases, namely a Pt rich disordered face centered cubic (fcc) phase “fcc1” (82–85 at% Pt), an ordered face centered tetragonal (fct) Pt<sub>50</sub>Co<sub>50</sub> phase “fct”, and a Co-rich disordered fcc phase “fcc2” (57–77 at% Co). The composition of the phases was estimated using a linear relation between the lattice constants and composition of fcc disordered Pt-Co alloys [34,35,46,47]. Mean crystallite sizes of each phase were estimated to fall in the range of 3–5 nm. What sets the structure of the three catalysts apart is the relative distribution of the “fcc1”, the “fcc2” and the ordered “fct” phase: peak intensity ratios between the fcc(1 1 1) reflection and the fct(1 0 1) reflection (Fig. 1a–c and last two columns in Table 1) were taken to qualitatively assess the abundance of each phase relative to the other two phases for between-catalysts comparisons. The data in Table 1 shows that for catalyst 1 each

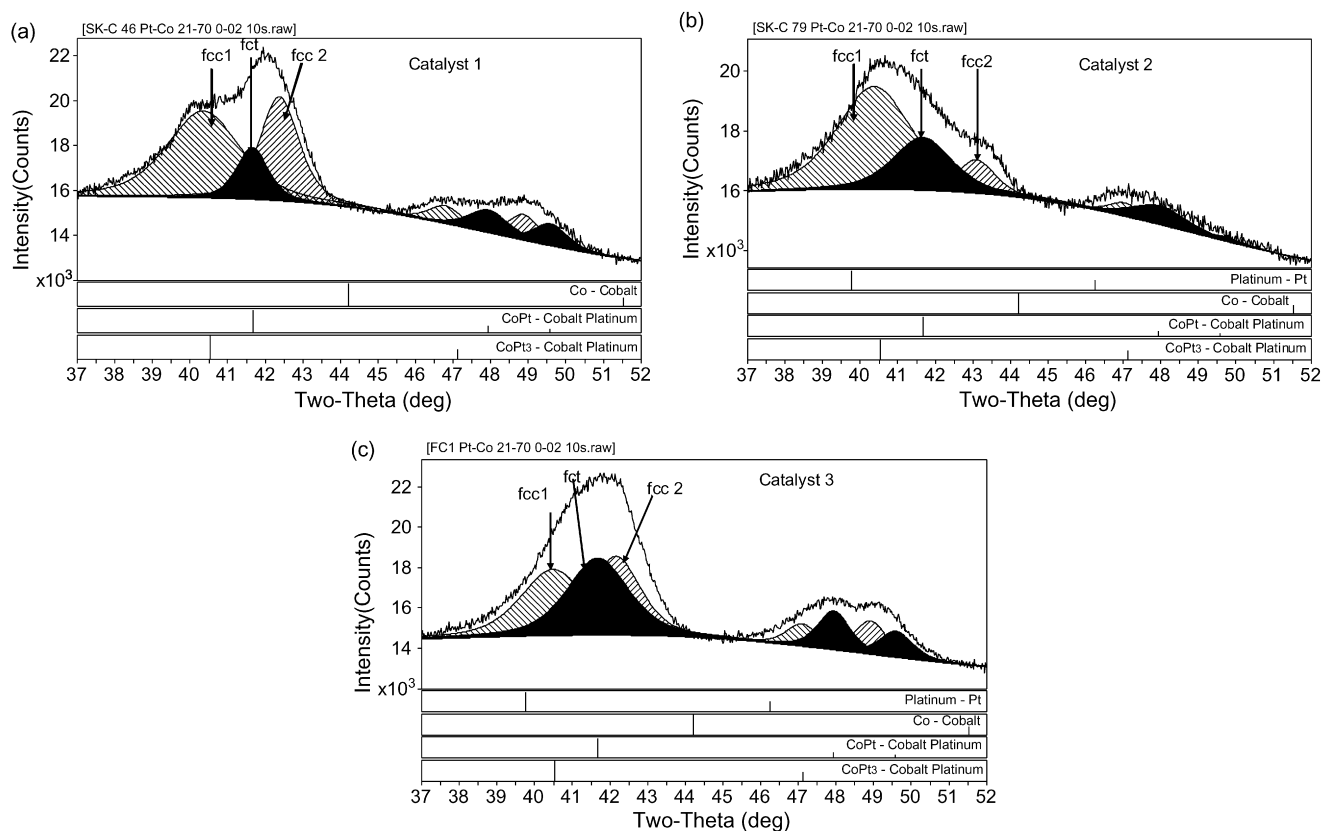


Fig. 1. (a) XRD profile and peak profile analysis of Pt<sub>50</sub>Co<sub>50</sub> electrocatalyst '1'. Two face disordered fcc (fcc1 and fcc2) and one ordered fct phases are present. The fcc1 and fcc2 phases outweigh the fct phase. (b) X-ray diffraction profile and peak profile analysis of Pt<sub>50</sub>Co<sub>50</sub> electrocatalyst '2'. Two face-disordered fcc (fcc1 and fcc2) and one ordered fct phases are present. The fct phase outweighs fcc2, but not fcc1. (c) XRD profile and peak profile analysis of Pt<sub>50</sub>Co<sub>50</sub> electrocatalyst '3'. Two face-disordered fcc (fcc1 and fcc2) and one ordered fct phases are present. The fct phase outweighs fcc1, and is about equal to fcc2.

of the two disordered phases clearly outweighs the ordered phase. Catalyst 2 exhibits the highest abundance in "fcc1", followed by "fct" and "fcc2". For catalyst 3, both relative peak intensity ratios are close to one (0.86 and 1.02) indicating the largest relative abundance of the "fct" phase among the three catalysts. The alloy phase distribution of catalyst 3 suggests the highest degree of alloying and can be rationalized by the fact that the 200 mg catalyst was annealed as a thin powder layer at the bottom of a large alumina dish with good exposure to

reducing hydrogen gas. Catalysts 1 and 2, which show less of the ordered phase, were both annealed in a small cylindrical quartz vial where the 200 mg of powder formed a layer of about 0.3 in. thickness. The distinct phase distributions of catalysts 1 and 2 despite almost identical preparation conditions demonstrate the sensitivity of the resulting alloy phase structure to the detailed preparation conditions. Considering the effect of slight variations in the annealing process on the observed alloy phase distribution for catalyst 3, we speculate that the alloy

Table 1

Overview of synthesis conditions, catalyst name, phase labels, crystallographic structural characteristics, and the relative peak intensities of the three Pt-Co electrocatalysts

Catalyst	Figure	Label	Alloy symmetry	Phase composition Pt:Co (at%:at%)	Lattice parameters, <i>a</i> / <i>c</i> (Å/Å)	Relative intensity of fcc1(1 1 1)/PtCo(1 0 1) peaks	Relative intensity of fcc2(1 1 1)/PtCo(1 0 1) peaks
1	Fig. 1a	fcc1	Disordered FCC Fm-3m	86:14	3.868/3.868	1.67	2.00
		fct	Ordered FCT P4/mmm	50:50	2.682/3.675		
		fcc2	Disordered FCC Fm-3m	39:61	3.691/3.691		
2	Fig. 1b	fcc1	Disordered FCC Fm-3m	85:15	3.867/3.867	1.95	0.63
		fct	Ordered FCT P4/mmm	50:50	2.682/3.675		
		fcc2	Disordered FCC Fm-3m	23:77	3.633/3.633		
3	Fig. 1c	fcc1	Disordered FCC Fm-3m	82:18	3.856/3.856	0.86	1.02
		fct	Ordered FCT P4/mmm	50:50	2.682/3.675		
		fcc2	Disordered FCC Fm-3m	43:57	3.709/3.709		

phase distribution is very sensitive to the detailed conditions of the annealing process. Minute variations in the solid state reduction and annealing process are therefore likely to account for the two distinct phase distributions in Fig. 1a and b.

While single phase Pt<sub>50</sub>Co<sub>50</sub> alloys were reported at temperature of about 900 °C [12] and 1–2 h, for the annealing temperatures (600 °C) and annealing times (7 h) reported here we mostly observe the formation of multiple Pt-Co alloy phases [25,26]. The opportunities of investigating multiple phase electrocatalysts have not been fully realized so far in the literature. Materials with multiple Pt-Co alloy phases offer the ability of a direct side-by-side comparison of the effect of ordering, lattice constant and composition of those alloy phases on electrochemical activity and alloy corrosion stability [25]. Also, multi-phase materials have proven more attractive over single phase materials in their electrochemical characteristics: comparative studies between Pt-Co alloy catalysts prepared at low and high annealing temperature have repeatedly shown that low temperature multi-phase materials can exhibit higher electrocatalytic ORR

activities compared to the high temperature material [25,26]. The concern over stability of the catalysts had also prompted stability tests for these Pt-Co alloy catalysts. Results of these tests can be found in a previous publication [25]. It was found that there exist strong effects of ordering on the stabilities of the different phases present in a low temperature Pt<sub>50</sub>Co<sub>50</sub> catalyst. The Co-rich disordered fcc phase was observed to be the most vulnerable to corrosion both during the preparation of the conducting polymer electrode layers and electrochemical measurements. However, it was also the phase that contributed to the greatest enhancement in catalytic activities with respect to pure Pt catalysts, as compared to the Pt-rich disordered fcc phase and the ordered fct phase.

### 3.3. Electrocatalytic activity and its relation to catalyst alloy structure

Fig. 2a shows the CV profiles of the three Pt-Co catalysts in deaerated solution after pretreatment but before ORR activity

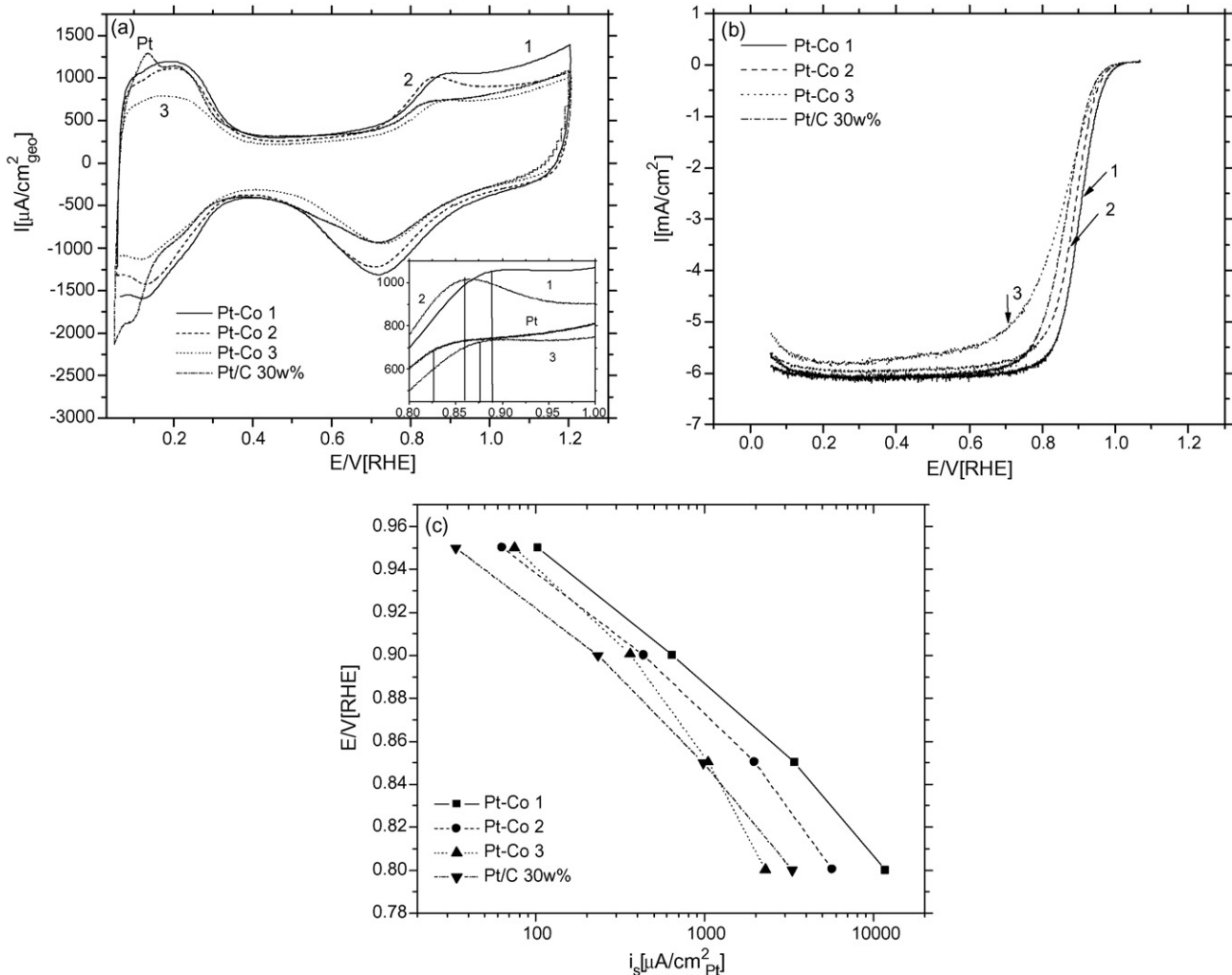


Fig. 2. (a) CV profiles ( $100 \text{ mV s}^{-1}$ ) of the Pt<sub>50</sub>Co<sub>50</sub> alloy catalysts '1', '2', and '3' after electrochemical preconditioning. For comparison the CV profile of the Pt reference catalyst is given. Inset shows a blow-up of the potential region where water activation and Pt–OH formation occur. (b) LSV ( $5 \text{ mV s}^{-1}$ ) of the three catalysts '1', '2', and '3' compared to a Pt reference catalyst. (c) Tafel plot of the Pt surface area normalized, mass transport corrected current density (specific activity) of the three Pt<sub>50</sub>Co<sub>50</sub> alloy catalysts compared to the reference Pt.

measurement in comparison to a pure Pt catalyst profile. The capacitive currents in the double layer regions are very similar for all three catalysts. The hydrogen ad- and desorption charge (0.05–0.4 V/RHE) and the corresponding ESA of catalysts 1 and 2 are very similar to that of the Pt reference catalyst. Catalyst 3, in contrast, exhibits a smaller hydrogen charge and consequently a reduced ESA. The latter finding may be explained considering the relative abundance between the “fcc1” phase and the other two phases of catalyst 3. The Co-rich phases “fct” and “fcc2” outweigh the “fcc1” phase, and the catalyst is therefore likely to expose fewer Pt atoms at the surface. The ESA values are also directly in line with earlier observations that ordered Pt-Co phases showed significantly reduced hydrogen adsorption characteristics [25,26] due to Co enrichment near the surface of the alloy particles [11,15].

Peaks at potentials between 0.7 and 0.9 V/RHE on the anodic scan are associated with water activation on the surface of Pt and Pt alloys, followed by the formation of oxygenated (hydroxides, oxides) surface species [48,49]. Between 0.6 and 0.8 V/RHE on the cathodic scan, these surface (hydr)oxides are reduced and a metallic surface is recovered. Catalysts 1 and 2 show a more pronounced faradaic formation and reduction of oxygenated species compared to Pt and catalyst 3. Considering that the ESA of the Pt catalyst and catalysts 1 and 2 are similar, this observation suggests that the surface of catalysts 1 and 2 forms a larger amount of oxygenated species, perhaps surface Co oxides or subsurface species, compared to pure Pt. The insert of Fig. 2a reports the relative peak positions of the surface oxide formation. All Pt-Co catalysts exhibit a peak shift in the oxide formation to more anodic potentials suggesting that the surface oxide coverage is reduced compared to pure Pt. According to a previously suggested kinetic model for the ORR [11,48], a reduced coverage of surface oxide species offers activity advantages due to higher oxygen chemisorption rates.

Fig. 2b reports the potential sweep voltammetry of all three catalysts in oxygen-saturated electrolyte. The geometric current density during  $5 \text{ mV s}^{-1}$  anodic sweeps is plotted against the applied potential. Catalysts 1 and 2 show significantly improved ORR reduction characteristics reaching the mass transport limiting current already at about 0.75 V/RHE. Catalyst 3 reaches the mass transport limited current at more cathodic potentials and the shape of its sweep resemble those observed for mainly ordered Pt-Co alloys [25,26], which is consistent with its alloy structure.

Fig. 2c illustrates the Tafel plots of catalysts 1, 2, 3, and of the pure Pt catalyst. The applied potential is plotted against the mass transport corrected ESA normalized current density (specific activity) of each catalyst in the kinetically controlled regime. Catalyst 1 shows the highest activities over the entire Tafel potential range. Catalysts 2 and 3 exhibit similar activities until about 0.9 V where catalyst 3 starts to deviate from the linear Tafel slope ( $-60$  to  $70 \text{ mV dec}^{-1}$ ) at high potentials. Deviation from linearity have been associated [11] with a gradual transition of the oxygen chemisorption from Temkin to Langmuir conditions. While Temkin conditions refer to oxygen chemisorption in the presence of oxygenated surface species stemming from water activation (see insert of Fig. 2a), Langmuir chemisorption

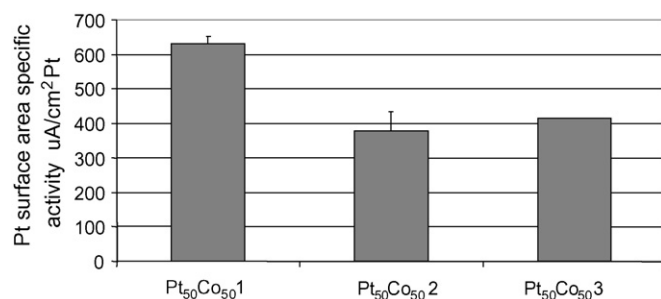


Fig. 3. Specific activities of the Pt<sub>50</sub>Co<sub>50</sub> alloy catalysts. The reference Pt electrocatalysts showed an activity of about  $200 \mu\text{A cm}^{-2} \text{Pt}$  at 900 mV/RHE. Error bars were determined from triplicate experiments.

occurs on mainly adsorbate-free surface and is associated with the ideal  $-120 \text{ mV dec}^{-1}$  Tafel slope.

Fig. 3 compares the activities of the three catalysts at 900 mV/RHE side by side. While catalysts 2 and 3 show a two-fold activity increase compare to Pt, catalyst 1 is over three times as active as the Pt catalyst.

Relating the structural and electrochemical characterization one can arrive at the following conclusions: prevalence of disordered Pt-Co alloy phases (catalyst 1), in particular the prevalence of a Co-rich “fcc2” phase, is associated with the largest activity gain for ORR compared to pure Pt. Prevalence of a Pt rich alloy (“fcc1”) phase diminishes the observed activity gains. Similarly, ORR activity gains over Pt are less pronounced if the ordered “fct” phase outweighs the disordered phases. Our analysis suggests that the Co-rich (60–80 at% Co) disordered alloy phase, “fcc2”, play a critical role in the observed ORR activity enhancements.

#### 4. Conclusions

We have addressed structural and electrocatalytic characteristics of three carbon supported high surface area Pt-Co alloy nanoparticle electrocatalysts of overall stoichiometry Pt<sub>50</sub>Co<sub>50</sub> for use as ORR electrocatalysts. A synthesis route was used that involved reductive thermal annealing and alloying in the solid state. Each catalyst consisted of a Pt rich (85–90 at%) disordered fcc Pt-Co alloy phase (“fcc1”), a Co-rich (60–80 at%) disordered fcc Pt-Co alloy phase (“fcc2”), and an ordered fct Pt<sub>50</sub>Co<sub>50</sub> alloy phase (“fct”). However, the relative distribution and abundance of the three Pt-Co alloy phases was distinctly different in each catalyst. The multi-phase nature of the catalysts has enabled a side-by-side assessment of the effect of the relative distribution of the phases on the electrocatalytic activity for ORR. The Co-rich disordered phase has been associated with the large activity gains of catalyst 1 compared to pure Pt. Prevalence of the ordered “fct” Pt<sub>50</sub>Co<sub>50</sub> phase over the Co-rich “fcc2” phase, independent of the relative abundance of the Pt rich phase, reduced the observed electrocatalytic activity for ORR. Based on a kinetic model for ORR, the activity enhancements are associated with the delayed formation of a complete layer of oxygenated surface species from water on the catalyst surface, resulting in a higher rate of oxygen adsorption and reaction.

Pt alloy electrocatalysts with multiple alloy phases, largely ignored in the literature to date, represent not only a very active class of catalytic materials but offer a unique opportunity to assess the relative stability and activity of individual alloy phases [25]. The presented results will be valuable in the design and search of more active Pt-Co ORR electrocatalysts.

## Acknowledgements

This project is supported by the Department of Energy under grant LAB04-20, Basic Energy Sciences, by the Texas Center for Superconductivity at the University of Houston, by the Center for Advanced Materials at the University of Houston, by the American Chemical Society Petroleum Fund, and by the seed grants (GEAR) provided by the University of Houston.

## References

- [1] P. Stonehart, *Phys. Chem.* 94 (1990) 913–921.
- [2] B.C. Beard, P.N. Ross, *J. Electrochem. Soc.* 137 (1990) 3368–3374.
- [3] F.J. Luczak, D.A. Landsman, Ternary Fuel Cell Catalysts Containing Platinum, Cobalt and Chromium US Patent 4,447,506 (1984).
- [4] F.J. Luczak, D.A. Landsman, Ordered Ternary Fuel Cell Catalysts Containing Platinum and Cobalt US Patent 4,711,829 (1987).
- [5] F.J. Luczak, D.A. Landsman, Ordered Ternary Fuel Cell Catalysts Containing Platinum and Cobalt and Method for Making the Catalyst US Patent 4,677,092 (1987).
- [6] E. Antolini, J.R.C. Salgado, M.J. Giz, E.R. Gonzalez, *Int. J. Hydrogen Energy* 30 (2005) 1213–1220.
- [7] E. Antolini, J.R.C. Salgado, E.R. Gonzalez, *J. Power Sources* 160 (2006) 957–968.
- [8] M.-k. Min, J. Cho, K. Cho, H. Kim, *Electrochim. Acta* 45 (2000) 4211–4217.
- [9] S. Mukerjee, S. Srinivasan, M.P. Soriaga, J. McBreen, *J. Electrochem. Soc.* 142 (1995) 1409–1422.
- [10] S. Mukerjee, S. Srinivasan, M.P. Soriaga, J. McBreen, *J. Phys. Chem.* 99 (1995) 4577.
- [11] U.A. Paulus, A. Wokaun, G.G. Scherer, T.J. Schmidt, V. Stamenkovic, V. Radmilovic, N.M. Markovic, P.N. Ross, *J. Phys. Chem. B* 106 (2002) 4181–4191.
- [12] L. Xiong, A. Manthiram, *J. Electrochem. Soc.* 152 (2005) A697–A703.
- [13] N. Travitsky, T. Ripenbein, D. Golodnitsky, Y. Rosenberg, L. Burshtein, E. Peled, *J. Power Sources* 161 (2006) 782–789.
- [14] U.A. Paulus, A. Wokaun, G.G. Scherer, T.J. Schmidt, V. Stamenkovic, N.M. Markovic, P.N. Ross, *Electrochim. Acta* 47 (2002) 3787–3798.
- [15] V. Stamenkovic, T.J. Schmidt, P.N. Ross, N.M. Markovic, *J. Phys. Chem. B* 106 (2002) 11970–11979.
- [16] V. Stamenkovic, B.S. Moon, K.J. Mayerhofer, P.N. Ross, N. Markovic, J. Rossmeisl, J. Greeley, J.K. Nørskov, *Angew. Chem. Int. Ed.* 45 (2006) 2897–2901.
- [17] H.A. Gasteiger, S.S. Kocha, B. Sompalli, F.T. Wagner, *Appl. Catal. B: Environ.* 56 (2005) 9–35.
- [18] A.S. Arico, A.K. Shukla, H. Kim, S. Park, M. Min, V. Antonucci, *Appl. Surf. Sci.* 172 (2001) 33–40.
- [19] A. Bonakdarpour, J. Wenzel, D.A. Stevens, S. Sheng, T.I. Monchesky, R. Lobel, R.T. Atanasoski, A.K. Schmoedel, G.D. Vernstrom, M.K. Debe, J.R. Dahn, *J. Electrochem. Soc.* 152 (2005) A61.
- [20] F.H.B. Lima, M.J. Giz, E.A. Ticianelli, *J. Braz. Chem. Soc.* 16 (2005) 328–336.
- [21] F.H.B. Lima, W.H. Lizcano-Valbuena, E. Teixeira-Neto, F.C. Nart, E.R. Gonzalez, E.A. Ticianelli, *Electrochim. Acta* 52 (2006) 385–393.
- [22] J.N. Soderberg, A.H.C. Sirk, S.A. Campbell, V.I. Birss, *J. Electrochem. Soc.* 152 (2005) A2017–A2022.
- [23] M. Teliska, V.S. Murthi, S. Mukerjee, D.E. Ramaker, *J. Electrochem. Soc.* 152 (2005) A2159–A2169.
- [24] L. Xiong, A. Manthiram, *J. Mater. Chem.* 14 (2004) 1454–1460.
- [25] S. Koh, J. Leisch, M.F. Toney, P. Strasser, *J. Phys. Chem. C*, in press.
- [26] S. Koh, M.F. Toney, P. Strasser, *Electrochim. Acta* 52 (2007) 2765–2774.
- [27] M. Watanabe, K. Tsurumi, T. Mizukami, T. Nakamura, P. Stonehart, *J. Electrochem. Soc.* 141 (1994) 2659–2668.
- [28] J.N. Soderberg, A.H.C. Sirk, S.A. Campbell, V.I. Birss, *Electrochem. Soc.* 152 (2005) A2017–A2022.
- [29] P. Strasser, Q. Fun, S. Gorer, M. Devenney, T. He, H. Oyanagi, D. Giaquinta, K. Urata, H. Fukuda, C. Konstantinos, *Platinum-Titanium-Tungsten Fuel Cell Electrocatalyst*, PCT Int. Appl. WO2004/109,829 (2004).
- [30] P. Strasser, S. Gorer, M. Devenney, H. Oyanagi, D. Giaquinta, K. Urata, H. Fukuda, K. Cendak, K. Chondroudis, *Platinum-Copper Fuel Cell Electrocatalyst*, PCT Int. Appl. WO2004/024,982 (2004).
- [31] P. Strasser, S. Gorer, M. Devenney, Q. Fan, K. Chondroudis, D. Giaquinta, T. He, H. Oyanagi, K. Urata, K. Iwasaki, H. Fukuda, *Fuel Cell Electrocatalysts of Pt-Mn-Co*, PCT Int. Appl. WO2003/073,541 (2003).
- [32] T.J. Schmidt, H.A. Gasteiger, G.D. Staeb, P.M. Urban, D.M. Kolb, R.J. Behm, *J. Electrochem. Soc.* 145 (1998) 2354–2358.
- [33] B. Merzougui, S. Swathirajan, *J. Electrochem. Soc.* 153 (2006) A2220–A2226.
- [34] L. Vegard, *Zeitschrift fuer Physik* 5 (1921) 2–26.
- [35] J. Friedel, *Phil. Mag.* 46 (1955) 514.
- [36] N. Travitsky, T. Ripenbein, D. Golodnitsky, Y. Rosenberg, L. Burshtein, E. Peled, *J. Power Sources* 161 (2006) 782–789.
- [37] A. Bauer, E.L. Gyenge, C.W. Oloman, *Electrochim. Acta* 51 (2006) 5356–5364.
- [38] S. Sun, S. Anders, T. Thomson, J.E.E. Baglin, M.F. Toney, H.F. Hamann, C.B. Murry, B.D. Terris, *J. Phys. Chem. B* 107 (2003) 5419–5425.
- [39] D.I. Garcia-Gutierrez, G.E. Gutierrez-Wing, L. Giovanetti, J.M. Ramallo-Lopez, F.G. Requejo, M. Jose-Yacamán, *J. Phys. Chem. B* 109 (2005) 3813–3821.
- [40] S. Sun, C.B. Murray, D. Weller, L. Folks, A. Moser, *Science* 287 (2000) 1989–1992.
- [41] C. Liu, X. Wu, T. Klemmer, N. Shukla, X. Yang, D. Weller, *J. Phys. Chem. B* 108 (2004) 6121–6123.
- [42] X. Yan, H. Liu, K.Y. Liew, *J. Mater. Chem.* 11 (2001) 3387–3391.
- [43] S. Koh, M.F. Toney, P. Strasser, *AICHE Fall Meeting*, San Francisco, 2006.
- [44] M. Hansen, *Constitution of Binary Alloys*, McGraw-Hill, New York, 1958.
- [45] D.A. Porter, K.E. Easterling, *Phase Transformations in Metals and Alloys*, Chapman and Hall, New York, 1992.
- [46] B.E. Warren, *X-ray Diffraction*, Reading, MA, 1969.
- [47] B.D. Cullity, S.R. Stock, *Elements of X-ray Diffraction*, 3rd ed., Prentice Hall, New York, 2001.
- [48] N.M. Markovic, P.N. Ross, *Surf. Sci. Rep.* 45 (2002) 117.
- [49] J. Lipkowski, P.N. Ross, *Electrocatalysis*, Wiley-VCH, New York, 1998.